

Design and Analysis of ANFIS controller Based multi-functional VSC for Grid connected solar PV-BES System

V. Venkata Harini¹ Mr. Ramu²

¹M.Tech Student, Department of Electrical and Electronics Engineering, Quba College of Engineering And Technology, Venkatachalam, Nellore, Andhra Pradesh, India

²Head of The Department , Department of Electrical and Electronics Engineering, Quba College of Engineering and Technology, Venkatachalam, Nellore, Andhra Pradesh, India

ABSTRACT

Article Info

Volume 9, Issue 4

Page Number : 140-151

Publication Issue

July-August 2022

Article History

Accepted : 02 July 2022

Published : 11 July 2022

In this review, a multifunctional Voltage Source Converter is utilized related to an Adaptive Neuro fuzzy inference System controller (ANFIS) to deliver a sun oriented Photovoltaic (PV)- battery energy storage based microgrid (VSC). This framework removes greatest power from a PV exhibit while additionally giving reactive power compensation, harmonics decrease, grid current adjusting, and a smooth progress from Grid Connected (GC) to Stand-Alone (SA) mode. This framework consequently changes to SA mode when the grid fails, ensuring that the load is provided without interference. At the point when the framework is reestablished, it changes to GC mode consequently. The VSC with ANFIS regulator capacities in current control in GC mode and voltage control in SA mode. This framework is fit for separating the best power from the sunlight based PV cluster whether or not it is in GC or SA mode. The charging and releasing of the battery is constrained by a bidirectional dc-dc converter. It sets the dc-connect voltage to the most extreme power point voltage of the PV exhibit. Assuming the battery is feeling the loss of, the control is right away moved to VSC for greatest power extraction from the PV cluster.

Keywords : Battery energy storage (BES), bidirectional dc-dc converter (BDDC), grid connected (GC) mode, power quality, solar photovoltaic (PV) array, standalone (SA) mode.

I. INTRODUCTION

Because of The Consumption of Customary Energy Sources and Their Effect on the Climate, The Utilization of Sustainable power Hotspots for Energy Creation Has Turned into A Favored Choice. Sun based energy age has become well known in contrast

with other energy sources because of its simplicity of accessibility, earth harmless nature, and diminishing patterns in the expense of sunlight based photovoltaic (PV) boards [1]. The major drawbacks of solar energy is that it is intermittent. As a result, the PV array cannot supply the load requirement at all times. The system's reliability suffers as a result of this. This challenge is

solved by combining a PV array with battery energy storage (BES) [2].

For coordinating the PV exhibit and BES into the electrical framework, there are various setups conceivable. A solitary stage matrix interfaced sunlight based PV-BES framework with maximal power extraction capacities has been distributed in the writing [3]. Most extreme power point following (MPPT) control, which creates obligation cycle for the dc-dc converter, is likewise recorded in the writing [4], where the extraction of greatest power from the PV cluster is accomplished by using MPPT control, which produces obligation cycle for the dc-dc converter.

The voltage source converter (VSC) is controlled with right control calculations to meet the power quality necessities. Most of the heaps associated at the normal coupling point are very inductive and nonlinear. The grid side's power factor is weak due to highly inductive loads, and nonlinear loads create considerable distortion in grid currents, which further distorts grid voltages. As a result, with a framework associated PV system, power quality improvement is basic. A distribution static compensator (DSTATCOM) is utilized to address power quality worries like harmonics, reactive power burden, and load unbalance, among others [5]–[7]. It is an appealing approach to load compensation over passive compensation due to its simplicity, speed, and soundness of activity. Since the DSTATCOM is a shunt-associated compensator, it works in current control mode. As a result, the generated reference currents determine DSTATCOM switching via an appropriate control approach. Researchers have used a variety of controls to improve power quality, including instantaneous reactive power theory [8], synchronous reference frame theory [9], instantaneous symmetrical component theory [10], least mean square (LMS), self-tuning filter, hyperbolic tangent function, digital disturbance estimator, and others. The speed with which the control algorithm responds to the unique condition with lesser weight

oscillation decides its adequacy. The VSC is controlled in the grid connected (GC) method of activity utilizing a leaky least mean mixed norm (LLMMN) versatile control. This control method allows for quick operation during a dynamic shift while keeping the predicted weight fluctuations to a minimal.

When the grid fails unexpectedly due to a malfunction in the system, the microgrid switches to standalone (SA) mode and operates independently of the main grid. That is, even if the main grid fails, the renewable energy source is able to supply the load requirement. As a result, power converters are critical in the microgrid for controlling power flow and managing power. The VSC operates in voltage control (VC) mode in SA mode. Even while the microgrid is operating in SA mode, the dc-interface voltage is kept up with at the PV array's most extreme power point (MPP) value, removing greatest power from the PV exhibit. The microgrid is resynchronized to the fundamental grid and works in GC mode after the reason for separation is distinguished. In the writing, some control calculations have been reported that have accomplished a consistent progress from GC to SA mode as well as the other way around.

The fundamental elements of the LLMMN with ANFIS-based PV-BES-based microgrid framework introduced in this article are greatest power extraction from the PV exhibit, grid current adjusting, unity power factor (UPF) activity at the network side, harmonics elimination, SA method of activity, and consistent change from GC to SA mode as well as the other way around.

Coming up next are the essential commitments of this examination project.

- 1) Greatest power from the PV array is removed, and power quality is worked on in a PV-BES-based microgrid.
- 2) Within the sight of BES, the bidirectional dc-dc converter (BDDC) extricates the greatest power from the PV array. At the point when the BES is eliminated from the microgrid, the VSC from the BDDC takes up the obligation of greatest PV power extraction.

- 3) A quick, oscillation-free LLMMN adaptive control supplies the switching pulses to the VSC, which compensates for the nonlinear load.
- 4) On the grid side, power quality is improved by keeping total harmonic distortions (THDs) in grid voltages and grid currents below 5%. As a result, it complies with IEEE 519.
- 5) Smooth transition of the microgrid from GC to SA mode when the grid fails, with reconnection to GC mode once the fault has been cleared.

II. SYSTEM CONFIGURATION

Fig. 1 shows a microgrid based on PV-BES. A PV array, a BES, a BDDC, a three-leg VSC, a three-phase system, and nonlinear loads are completely included. A solid state switch on the network side is utilized to accomplish grid outage and restoration. Ripple filters are utilized on both the grid and the load side to decrease voltage ripples. The charging and releasing of the BES is constrained by a BDDC. The changing signs to the VSC are produced by the ANFIS Regulator.

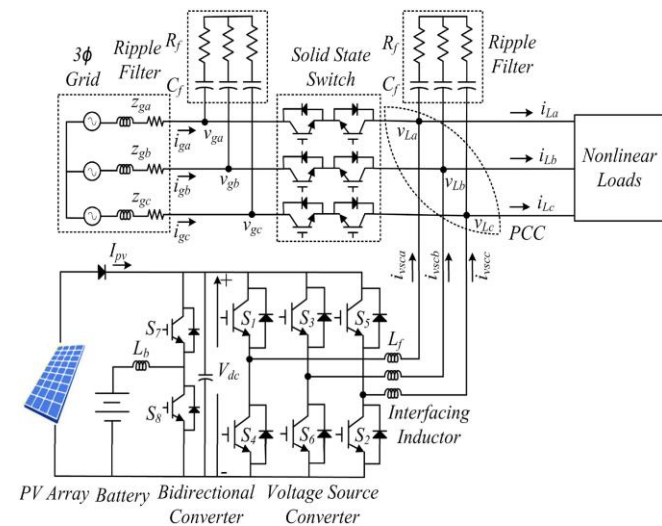


Fig. 1. Multifunctional PV-BES microgrid configuration.

III. CONTROL STRATEGY

The microgrids control approach is divided into four sections: MPPT control, VSC control, synchronization control, and BDDC control. The next sections go over these control strategies.

A. MPPT Control

Whether or not the framework is in GC or SA method of activity, the peak output from the sun oriented PV array should be removed. To augment PV exhibit use, the microgrid's PV array is run at its MPP in different atmospheric conditions. There are a few calculations for extricating the most extreme power from a PV exhibit, including irritate and notice (P&O), incremental conductance, fractional open-circuit voltage-based MPPT control, fractional short-circuit current-based MPPT control, and fuzzy control approach, which are all discussed in the literature. The PV array is controlled using P&O-based MPPT control to capture maximum power under variable sun irradiation.

B. VSC Control

This system has two methods of activity. At the point when the grid is available, one is in GC mode, and when the grid isn't, the other is in SA mode. Figure 2 shows the design of VSC control.

1. **GC Mode of Operation VSC Control:** In case BES is available in GC mode, VSC is utilized to convey a consistent capacity to the grid. For this situation, BDDC keeps the dc-connect voltage at the ideal level. In the event that the BES is absent in the system, the VSC regulates the dc-link voltage to the desired voltage, resulting in variable power feeding to or drawing from the grid based on PV generation and load demand. Figure 2 depicts the control of VSC in GC mode. The following are the main steps of VSC control in GC mode.

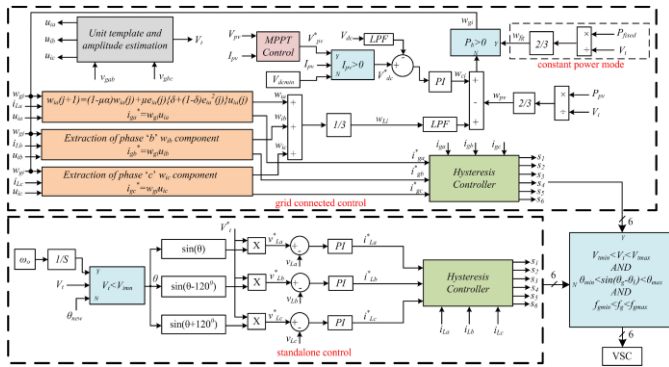


Fig. 2. VSC control algorithm in GC and SA mode

a). **Calculation of unit templates:** The grid phase voltages are estimated as follows:

$$V_{ga} = \frac{2V_{gab} + V_{gbc}}{3},$$

$$V_{gb} = \frac{-V_{gab} + V_{gbc}}{3}, V_{gc} = \frac{-V_{gab} - 2V_{gbc}}{3} \quad (1)$$

The sensed grid line voltages are V_{gab} and V_{gbc} . The mains voltages' amplitude (V_t) is as follows:

$$V_t = \sqrt{\frac{2}{3}(V_{ga}^2 + V_{gb}^2 + V_{gc}^2)} \quad (2)$$

The templates for the phased units are produced as follows:

$$u_{ia} = \frac{v_{ga}}{V_t}, u_{ib} = \frac{v_{gb}}{V_t}, u_{ic} = \frac{v_{gc}}{V_t} \quad (3)$$

b). **Calculation of active loss components:** In the GC method of activity, when the BES is absent, the VSC controls the dc-connect voltage to the ideal voltage; in any case, the BDDC manages the dc-interface voltage to the ideal voltage. The reference dc voltage (V_{dc}^*) comparable to the MPPT voltage is given by the MPPT control. Coming up next is a correlation of the reference dc-interface voltage (V_{dc}^*) with the distinguished dc-connect voltage (V_{dc}) at the jth moment:

$$V_{de}(j) = V_{dc}^*(j) - V_{dc}(j) \quad (4)$$

At the point when the PV array fails to produce power, the reference dc voltage (V_{dc}) unexpectedly changes from V_{pv} to a consistent dc values ($V_{dcmin} = 365$ V). Subsequently, the dc-interface voltage has no impact on the disturbance. A proportional-integral (PI) regulator is utilized to direct the dc interface voltage

by utilizing the error voltage (V_{pe}). Coming up next is the result of the PI regulator:

$$w_{ci}(j + 1) = w_{ci}(j) + K_{pd}(V_{de}(j + 1)) - V_{de}(j) + K_{id}V_{de}(j + 1) \quad (5)$$

The gains of the PI controller are where w_{ci} is the active loss component, and K_{id} s and K_{pd} s.

The gains of the PI regulator are the place where w_{ci} the active loss part, and K_{id} and K_{pd} s.

c). **Calculation of feed-forward components:** The feed forward part for consistent power taking care of mode, is given as follow

$$w_{fg} = \frac{2P_{fixed}}{3V_t} \quad (6)$$

Where the fixed power provided by the grid is P_{fixed} .

The power supply weight of the PV is as follows:

$$w_{pv}(j) = \frac{2P_{pv}(j)}{3V_t} \quad (7)$$

Where the power supply is provided by P_{pv} from the PV array.

d) **Basic active weight calculations of load currents:**

The basic active weight of phase 'a' load current with LLMMN adaptive control is shown

$$w_{ia}(j + 1) = (1 - \mu\alpha)w_{ia}(j) + \mu e_{ia}(j) * \{\delta + (1 - \delta)e_{ia}^2(j)\}u_{ia}(j) \quad (8)$$

Where $e_{ia}(j)$ the adaptive part error, μ is the progression size, α the spillage and μ the mixing boundary

$$e_{ia}(j) = i_{La}(j) - u_{ia}(j)w_{ia}(j) \quad (9)$$

Where the active weight, load current, and in-phase unit template "a" phase in the jth instant is $w_{ia}(j)$, $i_{La}(j)$, and $u_{ia}(j)$. The current active components of phase "b" and phase "c" are also evaluated as follows:

$$w_{ib}(j + 1) = (1 - \mu\alpha)w_{ib}(j) + \mu e_{ib}(j) * \{\delta + (1 - \delta)e_{ib}^2(j)\}u_{ib}(j) \quad (10)$$

$$w_{ic}(j + 1) = (1 - \mu\alpha)w_{ic}(j) + \mu e_{ic}(j) * \{\delta + (1 - \delta)e_{ic}^2(j)\}u_{ic}(j) \quad (11)$$

e) **Assessment of reference grid currents:** The performance of UPF on the grid side is investigated. The reference grid currents are generated in UPF operation by the use of the total w_{gi} active weight. The active weight of the grid depends on

TABLE I: Components In Active Weight of grid Currents

Mode of operation	Condition	Components Present in w_{gi}
Mode I – Fixed Power mode	Both solar PV array and BES are present	w_{fg}
Mode II – Fixed Power mode	Only BES present	w_{fg}
Mode III – Variable Power mode	Only solar PV array presents	$w_{Li} + w_{ci} - w_{pv}$
Mode IV – Variable Power mode(DSTATCOM operation)	Both Solar PV array and BES are absent	$w_{Li} + w_{ci}$

Various operating modes. Table I shows the active weight conditions in weight w_{gi} . Where w_{fg} w_{Li} is the average active load currents weight and is indicated as,

$$w_{Li} = \frac{(w_{ia}+w_{ib}+w_{ic})}{3} \quad (12)$$

The dc-link voltage is controlled by w_{ci} and the solar pv panel weight is w_{pv} . As weight w_{gi} multiplies with unit templates, the reference in-stage grid currents are obtained and given as following

$$i_{ga}^* = w_{gi}u_{ia}, i_{gb}^* = w_{gi}u_{ib}, i_{gc}^* = w_{gi}u_{ic}, \quad (13)$$

f) Generation of switching pulses: The VSC switching signals in GC mode are generated with error signals from the comparison of the reference grid currents (i_{ga}^* , i_{gb}^* , and i_{gc}^*) to the grid sensing currents (i_{ga} , i_{gb} , i_{gc}).

2) Control of VSC in SA Mode of Operation: The three-stage load voltages in SA mode are created as follows:

$$v_{La}^* = V_t^* \sin(w_0 t), v_{Lb}^* = V_t^* \sin\left(w_0 t - \frac{2\pi}{3}\right), v_{Lc}^* = V_t^* \sin\left(w_0 t + \frac{2\pi}{3}\right) \quad (14)$$

Where V_t^* is the magnitude of the voltages reference, and where w_0 the 314 rad /s is

Nominal frequency. In correlation with the sensed load voltages (v_{La} , v_{Lb} , v_{Lc}) and PI regulators are given the reference voltages (v_{La}^* , v_{Lb}^* , v_{Lc}^*). The result

of PI regulators are the benchmarks for load currents (i_{La}^* , i_{Lb}^* , i_{Lc}^*). Correlation with the detected load currents (i_{La} , i_{Lb} , i_{Lc}) and the results are supported by a hysteresis regulator for generating the VSC pulses in the SA mode. Figure 2 shows the block diagram of the SA mode control of the VSC. If V_t magnitude of the grid phase voltage exceeding V_{tmin} , the angle of the reference voltage phase θ_{new} is replaced with alternatively for the synchronization of the grid. The new signal generation θ_{new} is illustrated in Fig. 3. (a).

C. Synchronization Control

Figure 3 shows the synchronization control (b). The magnitude of the grid voltage and the difference between

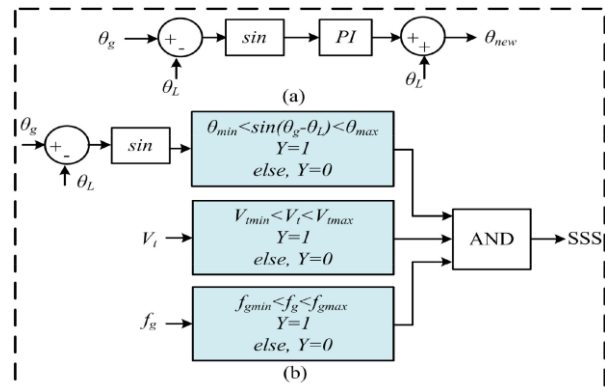


Fig. 3. (a) And (b) Synchronization control.

Angle (θ_g and load phase angle (θ_L), the grid frequency (f_g) is checked for inside endorsed limits. On the off chance that the conditions are satisfied, the AND Gate yield is "1" and the strong state switch showed in Figure 1 is shut, the network is associated with the framework and the VSC works in GC functional mode. At the point when a portion of the conditions are not met, the AND door yield becomes "0," so the strong state switch is left open, while the SA control is applied to VSC.

D. BDDC Control

Figure 4 shows the control for the BDDC. The correlation of the voltage dc-connect (V_{dc}^*) to the detected voltage dc-interface (V_{dc}) gives a error signal and is taken care of into a PI regulator. The dc-connect voltage is controlled utilizing this PI regulator to the desired value. It is contrasted with the

detected battery (I_b), and the subsequent sign is given to an alternate PI controls. the power supplied to the PI control is a reference battery current (I_b^*). This results in the BDDC duty cycle. The pulsewidth modulation signals for the BDDC are provided by the comparison of this duty signal with the Sägetooth wave.

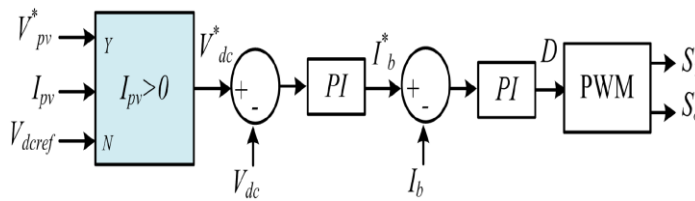


Fig. 4. BDDC control

E. ANFIS Controller

We designed the ANFIS regulator in Matlab/Simulink programming has displayed in fig 5. ANFIS can be prepared 100 epochs the error tolerance set to 0.01 can be streamlined by utilizing hybrid control strategy. The training error and ANFIS structure have displayed in roar fig6 and fig7..

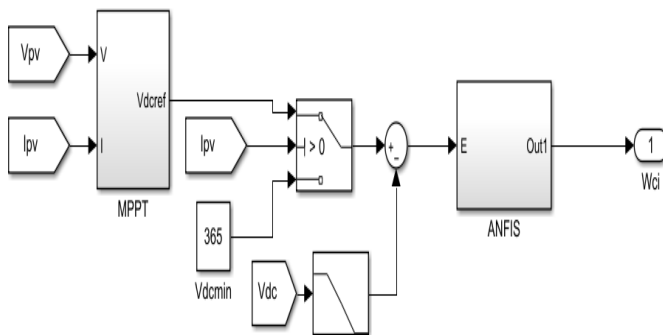


Fig5. Block diagram of ANFIS Controller

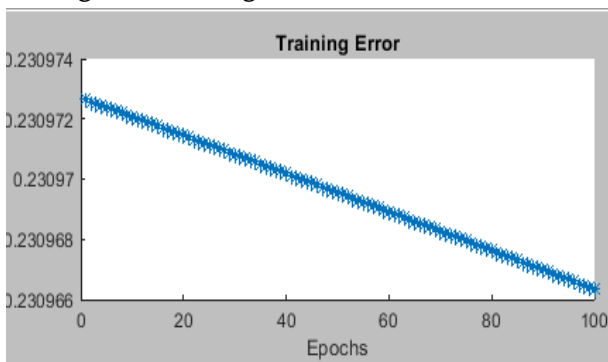


Fig.6: Training error versus epochs for the ANFIS.

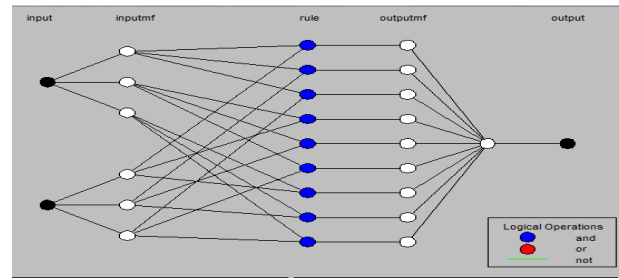


Fig.7: ANFIS-based MPPT structure

As part of the ANFIS controller, there are three membership functions and nine rules. Figures 8 and 9 show the ANFIS membership functions. For each of the two ANFIS factors, phonetic factors, such as Low, Medium, and High, are transmitted. If (e) and (de) are both high, a lead in the run base can be stated in the following way: (output is high). We use a system that is based on rules. According to the ANFIS's adjustments role, the administer base changes the duty cycle of the voltage source converter to PWM. The standards can be configured anyway you want. The three membership function elements of the error and the correction in error each have nine rules.

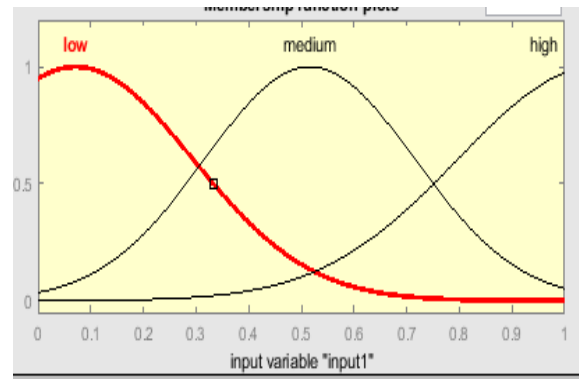


Fig.8: Error Member ship functions

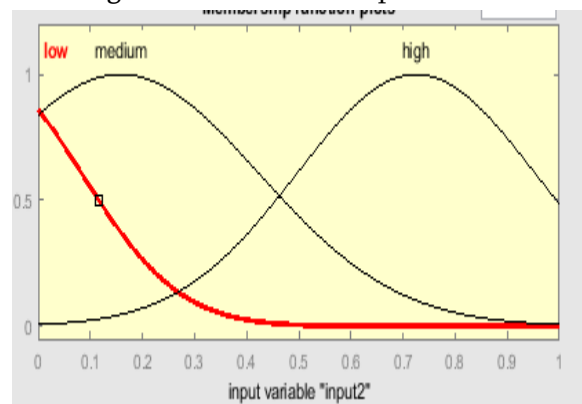


Fig.9: Change in error Member ship functions

In comparison to previous control techniques, the suggested ANFIS is faster and easier to use. The ANFIS editor's nine rules are listed in Table 2 below.

Table2: rules for ANFIS controller

$e/\Delta e$	<i>Low</i>	<i>Medium</i>	<i>High</i>
<i>Low</i>	<i>Low</i>	<i>Medium</i>	<i>High</i>
<i>Medium</i>	<i>Medium</i>	<i>High</i>	<i>High</i>
<i>High</i>	<i>High</i>	<i>High</i>	<i>High</i>

IV. SIMULATION RESULTS

MATLAB/Simulink toolbox is used to study simulated performance of the microgrid. Leistung is evaluated at a line voltage of 230 V, 50 Hz in various operating conditions.

4.1 simulation results using PI controller

A. Steady-State Performance in GC Mode

Fig. 10 shows the microgrid's steady state performance in GC working mode. It shows network voltages, grid currents, load current, VSC current, power supply, current and voltage photovoltaic array, system power, load power, PV power and battery power. It shows that the VSC injects the secluded currents to keep system currents sinusoidal. Grid currents with network voltages are 180° out of the phase, as constant power is provided to the framework.

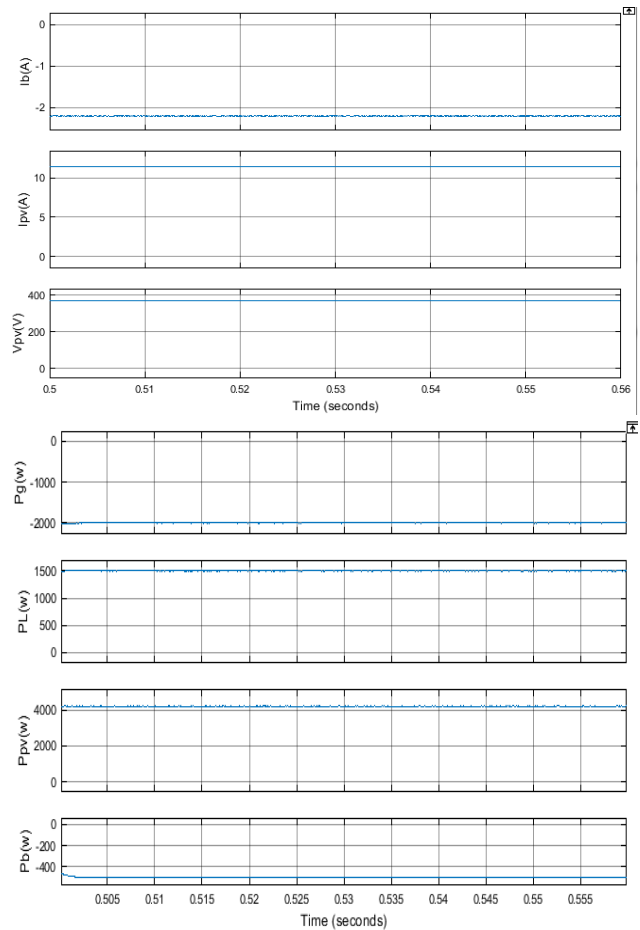
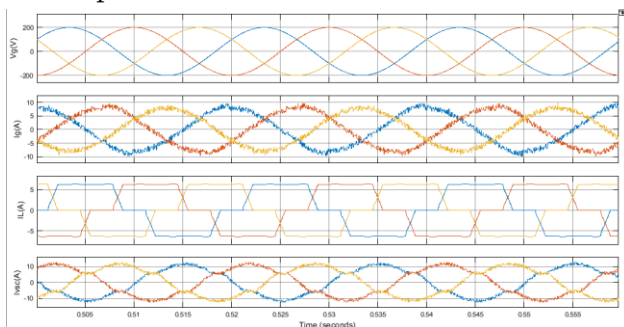


Fig.10. Steady state operation of the microgrid in GC mode.

B. Steady-State Performance in SA Mode

Fig. 11 shows the micro grid's static presentation in SA mode. It shows charging voltages, battery power, photovoltaic current and voltage cluster, photovoltaic output power, power and load power. The ideal frequency is accomplished by a proper SA control calculation for sine, adjusted, and desired voltages. By controlling the BDDC, the dc-connect voltage is controlled to the ideal voltage. The productivity of the radiation is examined at 1000 W/m2. At this illumination the power output of the PV array is 4.1 kW. The load requires a power of 1.5 kW. The PV array satisfies the need for load and the remainder of the energy in the battery is put away.

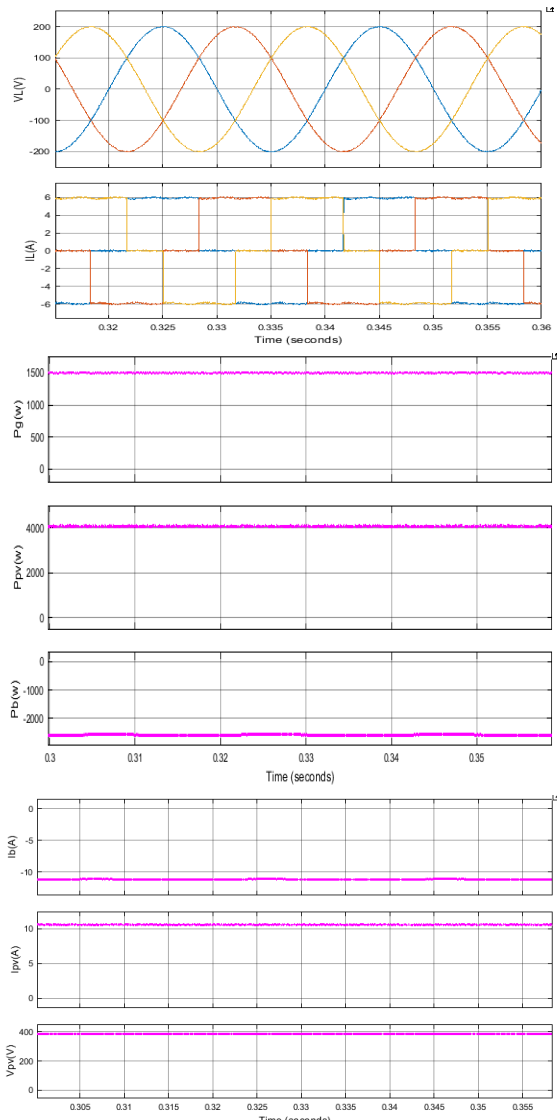


Fig. 11. Steady-state operation of the microgrid in SA mode.

C. Dynamic Performance of Microgrid at Change in Level of Solar Irradiation

Figure 12 represents the micro grid's exhibition for various sun oriented illumination. The presentation incorporates grid voltage, grid current, load flows, VSC current, battery current, PV way current and pressure, system energy, load power, PV way, and battery limit. The presentation of the sunlight based radiation at 0.7sec is examined by decreasing from 1000 to 500 W/m².

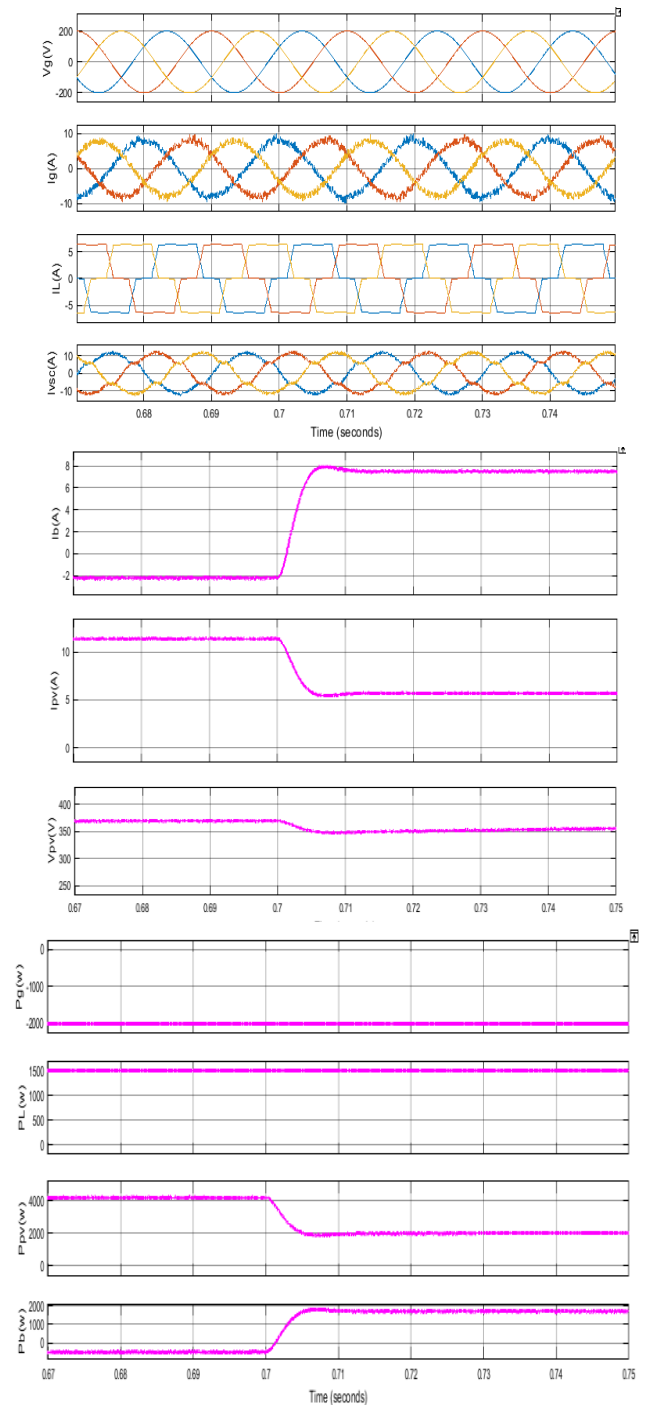


Fig. 12. Performance of microgrid under a Change in the level of solar irradiation.

D. Seamless Operation of Microgrid from GC Mode to SA Mode

Fig. 13 shows the consistent microgrid transmission from GC to SA mode. It shows the three-stage grid voltage and charge voltage, the system currents, the load currents, the VSC, the network and load voltages

stage points, the PV and current exhibit voltage and battery power. A fixed power is provided into the grid in GC mode. The grid voltages become zero when the primary network is separated. In this manner the VSC SA control is turned on and meets the load requirements.

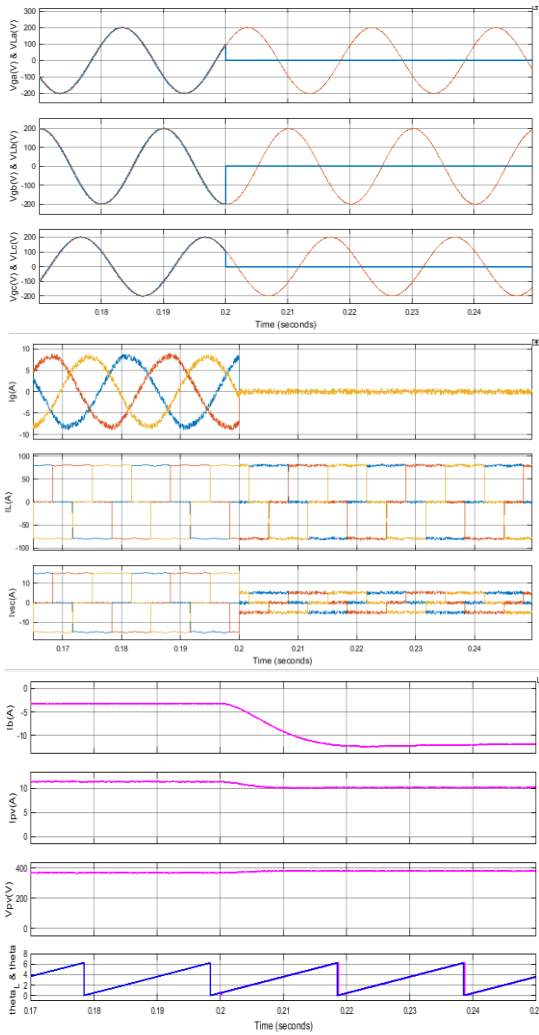
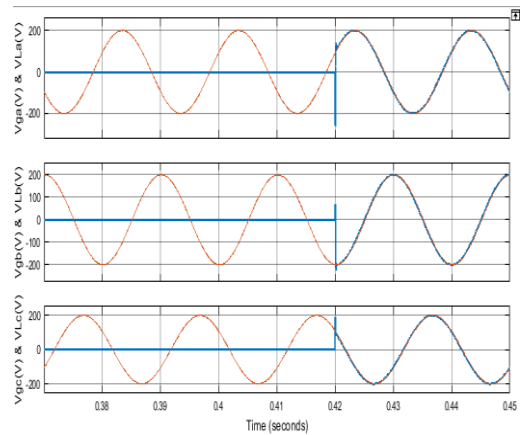


Fig. 13. Seamless transition of microgrid from GC mode to SA mode.

F. Seamless Operation of Microgrid From SA Mode to GC Mode

Figure 14 shows the micro grid’s consistent exchanges from SA to GC mode. It shows three stage grid voltage and load voltage, network currents, load voltage and currents, VSC voltages and currents, framework and load strain stage points, PV voltage and current

exhibits and the battery current. Toward the start, the SA mode is utilized for the microgrid



The framework is recovered at 0.4 s. In any case, when the voltages, frequencies, and stage points are in as far as possible, the essential system is simply associated with the microgrid. At first, the load pressure stage points and the net strain are grid up. The stage points of the lattice pressures and burden strains are 0.42 s individually. This implies that the fixed number of strands is just 0.42 s into the grid.

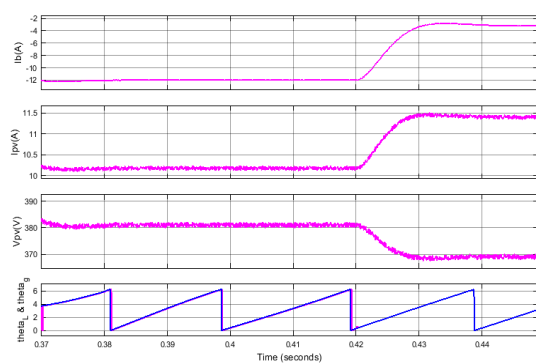
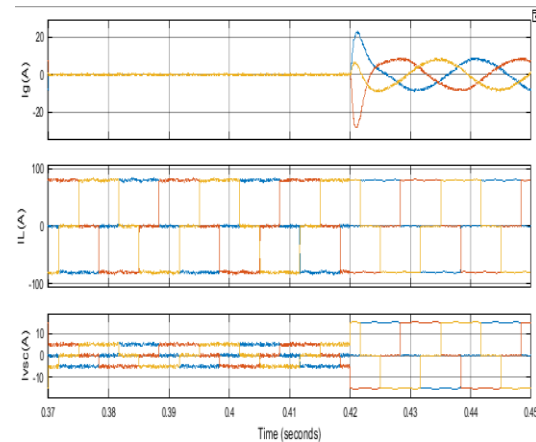


Fig. 14 Seamless transition of microgrid From SA mode to GC mode.

4.2 Simulation results using ANFIS Controller:

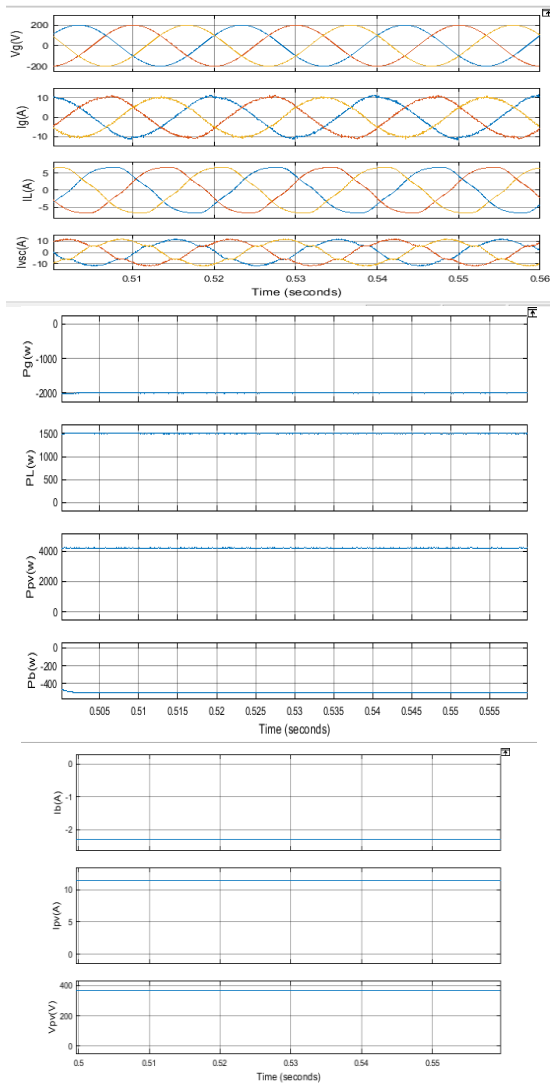


Fig. 15. Steady-state operation of the Microgrid in GC mode.

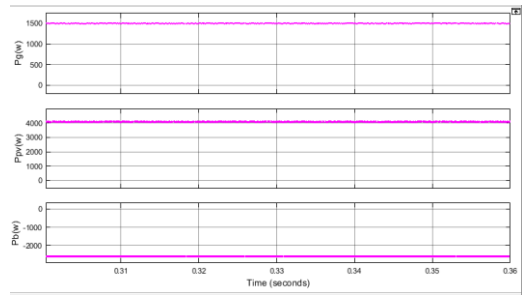
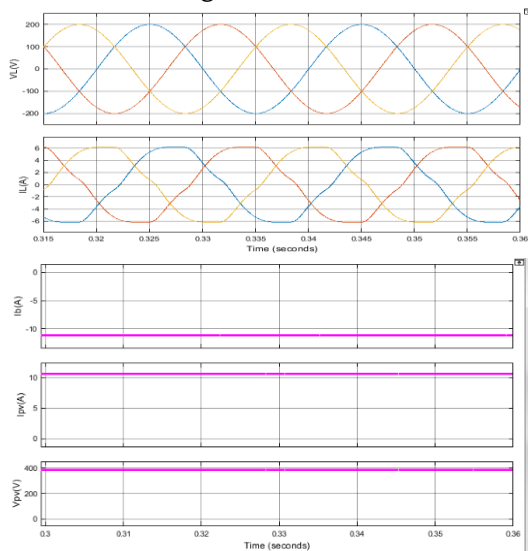


Fig. 16. Steady-state operation Of the microgrid in SA mode

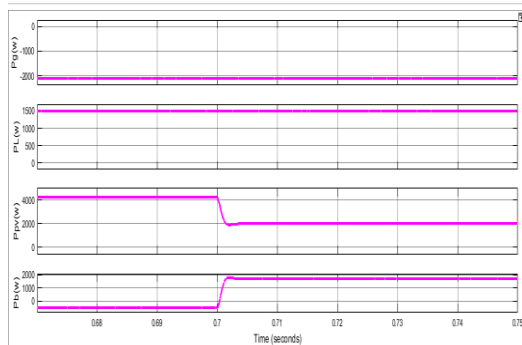
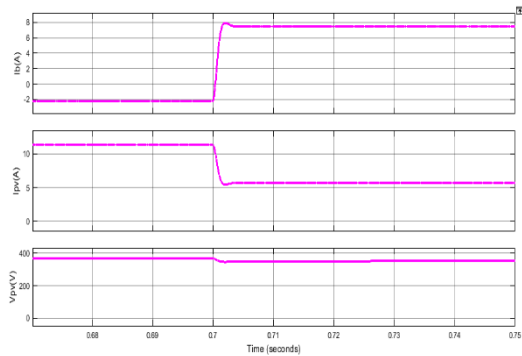
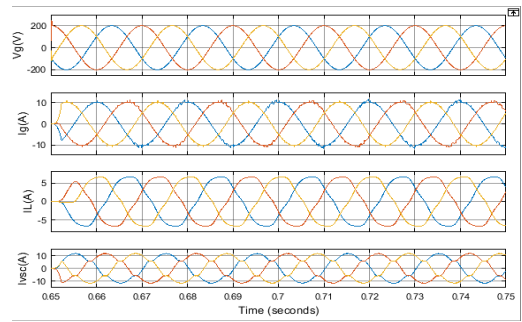
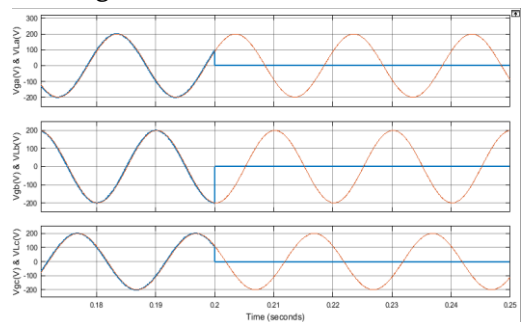


Fig. 17 Performance of microgrid under a Change in the level of solar irradiation.



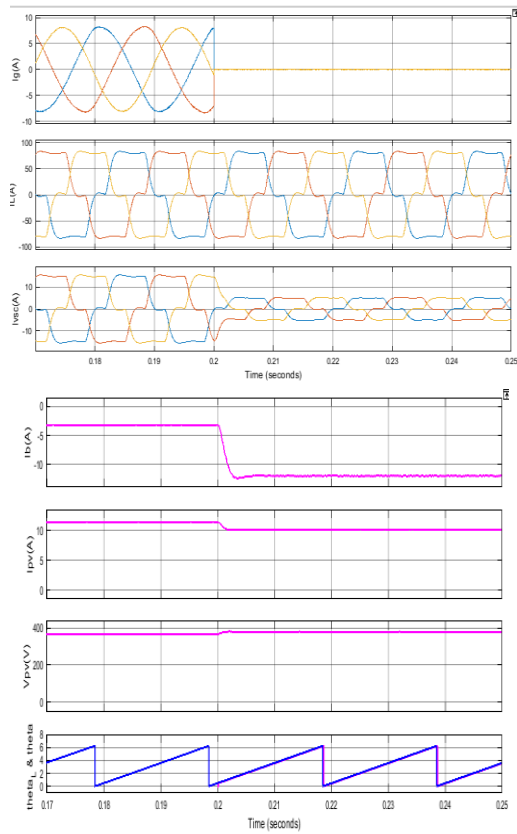


Fig. 18. Seamless transition of microgrid from GC mode to SA mode.

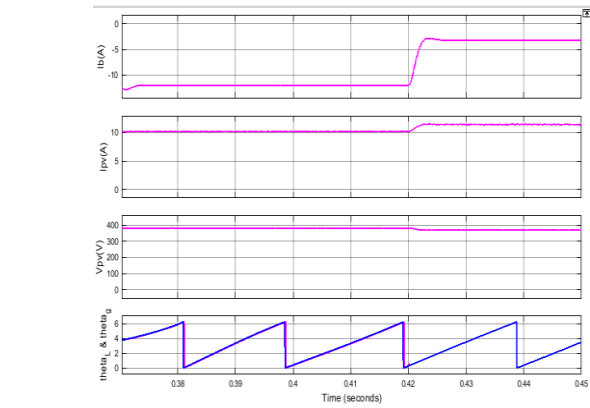
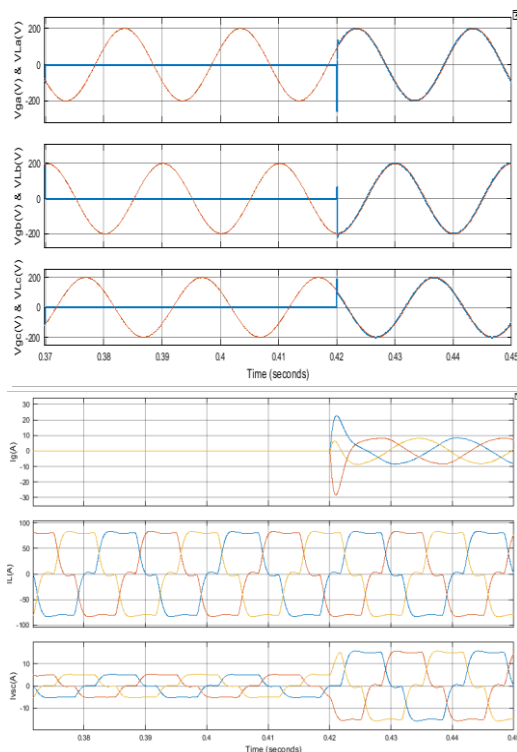


Fig. 19. Seamless transition of microgrid from SA mode to GC mode.

Table: 3 THD comparison table

method	parameter	GC mode	SA mode	Change in radiation
PI	Load current	21.65%	31.08%	21.67%
NN	Load current	3.68%	4.94%	4.32%

IV. CONCLUSION

The operation of the microgrid in several modes is investigated in this study, revealing the system's multifunctional capabilities. This system can work in both GC and SA modes without upsetting load supply, and it can change from GC to SA mode as vice versa with ease. A BDDC gathers the best power from the sun based PV array when the BES is turned off with system execution. At the point when the BES is turned off, the MPPT control is moved to VSC with ANFIS control, ensuring that the PV array is continually working at MPP. According to the comparative study, the suggested LLMMN with ANFIS control surpasses the traditional LMMN with PI control and LMS controls. The suggested LLMMN with ANFIS control has lower THD values than typical LMMN with PI control and LMS controls, resulting in a lower steady state error.

V. REFERENCES

- [1]. E. Goutard, "Renewable energy resources in energy management systems," in Proc. IEEE PES Innovative Smart Grid Technol. Conf. Europe, 2010, pp. 1–6.
- [2]. P. Andea, A. V. Mnerie, F. Solomonesc, O. Pop, and D. Cristian, "Conventional vs. alternative energy sources overview. Part II. European strategies," in Proc. Int. Joint Conf. Comput. Cyber. Tech. Informat., 2010, pp. 601–606.
- [3]. B. S. Shatakshi and S. Mishra, "Dual mode operational control of single stage PV-battery based microgrid," in Proc. IEEMA Eng. Inf. Conf., 2018, pp. 1–5.
- [4]. N. Saxena, I. Hussain, B. Singh, and A. L. Vyas, "Solar PV interfaced to multifunctional VSC with a battery support," in Proc. IEEE Power India Int. Conf., 2016, pp. 1–6.
- [5]. B. Singh, A. Chandra, and K. Haddad, *Power Quality: Problems and Mitigation Techniques*. New Delhi, India: Wiley, Jan. 2015.
- [6]. B. Singh, P. Jayaprakash, D. P. Kothari, A. Chandra, and K. A. Haddad, "Comprehensive study of DSTATCOM configurations," *IEEE Trans. Ind. Informat.*, vol. 10, no. 2, pp. 854–870, May 2014.
- [7]. M. BarghiLatran, A. Teke, and Y. Yolda,s, "Mitigation of power quality problems using distribution static synchronous compensator: A comprehensive review," *IET Power Electron.*, vol. 8, no. 7, pp. 1312–1328, Jul. 2015.
- [8]. N. D. Tuyen and G. Fujita, "PV-active power filter combination supplies power to nonlinear load and compensates utility current," *IEEE Power Energy Technol. Syst. J.*, vol. 2, no. 1, pp. 32–42, Mar. 2015.
- [9]. V. Narayanan and P. Jayaprakash, "Performance comparison of threephase four-wire grid integrated solar photovoltaic system with various control algorithms," in Proc. Int. Conf. Intell. Comput.,Instrum. Control Technol., 2017, pp. 406–414.
- [10]. M.V. ManojKumar, M. K. Mishra, and C.Kumar, "A grid-connected dual voltage source inverter with power quality improvement features," *IEEE Trans. Sustain. Energy*, vol. 6, no. 2, pp. 482–490, Apr. 2015.

Authors profile:

V VENKATA HARINI currently Pursuing Post Graduation at QUBA COLLEGE OF ENGINEERING AND TECHNOLOGY,



M.Ramu received graduate degree in electrical and electronics engineering in Sri SKR college of Engineering and Technology manubolu, SPSR Nellore district and post graduation degree specialisation of electrical power systems in N.B.K.R Institute of Science and Technology Vidyanagar, Nellore and presently working as assistant professor in EEE Department At QUBA College Of Engineering And Technology Venkatachalam, Nellore A.P

Cite this article as :

V. Venkata Harini, Mr. Ramu, " Design and Analysis of ANFIS controller Based multi-functional VSC for Grid connected solar PV-BES System", *International Journal of Scientific Research in Science and Technology(IJSRST)*, Print ISSN : 2395-6011, Online ISSN : 2395-602X, Volume 9, Issue 4, pp.140-151, July-August-2022.
Journal URL : <https://ijsrst.com/IJSRST229420>